IEEE Access
Multidisciplinary | Rapid Review | Open Access Journal

Received August 6, 2021, accepted August 25, 2021, date of publication August 31, 2021, date of current version September 9, 2021.

Digital Object Identifier 10.1109/ACCESS.2021.3109267

Investigation and Analysis of Novel Skewing in a 140 kW Traction Motor of Railway Cars That Accommodate Limited Inverter Switching Frequency and Totally Enclosed Cooling System

HYUNGKWAN JANG[1], HYUNWOO KIM[1], DONG-WOO NAM[2], WON-HO KIM[2], JU LEE[1], (Senior Member, IEEE), AND CHANGSUNG JIN[3]

[1]Department of Electrical Engineering, Hanyang University, Seoul 04763, Republic of Korea
[2]Department of Electrical Engineering, Gachon University, Seongnam-si, Gyeonggi-do 13120, Republic of Korea
[3]Department of Electrical Engineering, Wonkwang University, Iksan, Jeollabuk-do 54538, Republic of Korea

Corresponding author: Changsung Jin (csjin76@wku.ac.kr)

This work was supported in part by Basic Science Research Program through the National Research Foundation of Korea(NRF) funded by the Ministry of Education(No. 2019R1F1A1060843), and in part by the National Research Foundation of Korea(NRF) grant funded by the Korea government(MSIT) (NRF-2020M3H4A3106183).

ABSTRACT This study facilitated the improvement of no-load back electromotive force (back-EMF) wave form, total harmonic distortion (THD) of back-EMF, and torque ripple using a novel skew angle formula, considering the specific order of a no-load THD. In real usage environments, it is taken into consideration for the fully enclosed cooling system and limited inverter switching frequency of urban railway car traction motors. Since the most railway car traction motors use high-withstand voltage rectangular wires in slot-open structure, a no-load back EMF waveform includes large space slot harmonics, which should be smaller as possible. For 6-step control, the no-load back EMF waveform is important because switching for motor control is performed once after the rotor position is determined. To improve the no-load back EMF waveform and THD, two-dimensional and three-dimensional finite element analysis (FEA) were performed using a novel skew angle formula considering specific harmonic order reduction, while the fundamental amplitude was minimally reduced. A prototype with the novel skew was fabricated and verified. In addition, it was designed by calculating a low current density for a fully enclosed cooling system. A temperature saturation experiment was also performed, and successfully verified. Therefore, we suggest that the no-load back EMF characteristics and torque ripple are improved by applying the novel skew angle instead of a traditional skew angle.

INDEX TERMS Current density, no-load back-electromagnetic force (EMF) wave, railway car traction motors, skew angle, 6-step control.

I. INTRODUCTION

The global railway market is gradually increasing. There are various railway systems, from low-speed railways operating in cities to high-speed railways connecting countries. Traction motors, which are the most important technology in railway systems, are classified into two: rotating motor type and linear motor type [1]. The rotating motor type is most commonly used in traditional railway, whereas the linear type is applied to ultra-high speed maglevs [2], or mid-and-low speed maglevs [3]. Rotating motors can be further classified into rigid-axle wheelset types that drive a wheel connected to one shaft with a single motor and independently rotating wheel types that control each wheel [4], [5]. Among the different traction types of railway vehicles, a rotating motor type with a rigid-axle wheelset structure is the most preferred type.

In the case of railway car traction motors, many countries require the reliability, stability, and high efficiency for railway vehicle components [6]–[8]. Also, traction motors are a considerably more environmental friendly system than combustion engines because they cause less pollution [9]–[11]. Interior permanent magnet synchronous motors (IPMSMs) are now being gradually expanded and used for traction of

The associate editor coordinating the review of this manuscript and approving it for publication was Philip Pong.

a railway car [12], [13]. The traction motor consumes the most electricity in the railway system, which necessitates a highly efficient motor to save energy [14]. The conventional induction motor (IM) for railway car traction is equipped with a semi-closed cooling system, which requires periodic maintenance, inspection, air ducts and an external fan [15]. The IM is less costly and easier to manufacture than permanent magnet synchronous motors (PMSM). However, it has the disadvantage of a low starting torque and a slow response rate, owing to its inherent dynamic characteristics. PMSM is advantageous in terms of its quick response because it has fast dynamic characteristics with high power density and efficiency [11], [16], [17]. In addition, considering the maintainability and reliability of the motor, a fully enclosed cooling system is suitable and possesses excellent vibration and noise characteristics [18]. Furthermore, a fully enclosed cooling system has the advantage of low maintenance costs, as it does not require periodic maintenance.

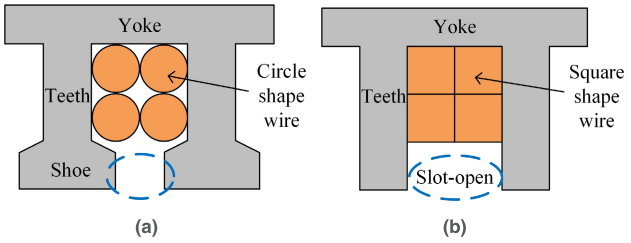

FIGURE 1. Stator slot shape: (a) shoe type with circle shape wire (b) slot-open type with square shape wire.

The PMSM controller requires rotor position information. The switching frequency of the inverter must be such that it switches at least 10 times within an electrical angle of the motor. However, there is a limit to controlling the six-pole traction motor using the space vector pulse width modulation (SVPWM) method with the limited switching frequency of the currently used inverter. In the case of switching at least 10 times per electrical angle using the double sampling method, the SVPWM can be applied for the six-pole traction motor up to 3200 rpm. Therefore, a 6-step control is required. In a 6-step control, only one switching is performed per electrical angle, which requires accurate waveform of no-load back electromotive force (EMF). If there is a difference between voltage command values and the sensed voltage values according to the rotor position, the torque ripple becomes severe. Hence, it is necessary to create the no-load back-EMF waveform to resemble a sine wave by minimizing the total harmonic distortion (THD) of the no-load back EMF as much as possible. However, while using a square winding with a high fill factor as shown in Fig. 1, the slot-open structure must be utilized as it has a large slot harmonic component and a large torque ripple. The torque ripple can be a source of vibration and acoustic noise [19]–[23]. Vibration in railway vehicles makes passengers uncomfortable [24]. Therefore, for the traction motor, it is necessary to design the no-load back-EMF and torque ripple as small as possible so that passengers experience a comfortable ride [25]. One of the methods to reduce the no-load back EMF THD is to apply a skew to the stator or rotor [26]. However, the skew also reduces the magnitude of the fundamental amplitude, which tends to decrease the motor power [27]. In this study, a novel skew angle formula has been introduced, where the magnitude of the fundamental amplitude decreases minimally. Moreover, as the new skew angle formula considers a specific harmonic order, it was confirmed that its reduction effect was considerable.

However, the fully enclosed cooling system is disadvantageous in terms of cooling performance, because outside air is not circulated inside the motor. In order to prevent an insulation breakdown, it is necessary for the motor to self-regulate the amount of heat generated by it. Hence, it is imperative to design the current density of the motor as low as possible.

In this study, the design of a novel skew angle formula that considers the controllability and fully enclosed cooling system, were conducted through a 2-D and 3D finite element analysis (FEA).

TABLE 1. Specification of a 140 kW IPMSM for a urban railway traction motor.

Item	Quantity	Unit
Stator outer diameter	500	mm
Rotor outer diameter	300	mm
Stack length	220	mm
Magnet size (length/thickness)	32 / 12	mm
Magnet grade	Sm_2Co_{17}	
Turns per slot	8	turn
Parallel branches	2	-
Input current (Continuous rate / 1-hour rate)	116 / 170	A_{rms}
Coil size	4 x 5.1	mm^2

II. ANALYSIS OF A NO-LOAD BACK EMF IN A SLOT-OPEN STRUCTURE BASED ON THE USE OF RECTANGULAR WINDING

A. SPECIFICATION OF AN URBAN RAILWAY TRACTION MOTOR

The traction motor for urban railway cars is designed to accommodate both empty cars and full load cars. Empty cars have a continuous rate of power of 140 kW, for which the required average torque is 610 Nm at 2200 rpm, where as a full load car is a 1-hour rate of power of 210 kW, for which the required average torque is 920 Nm at 2200 rpm. The required torque at the continuous rated maximum speed is 280 Nm, whereas the required torque at the 1-hour rated maximum speed is 437 Nm. The maximum speed is 4810 rpm. On application of a fully enclosed cooling system, the current density was calculated to be 2.84 A_{rms}/mm^2. The design

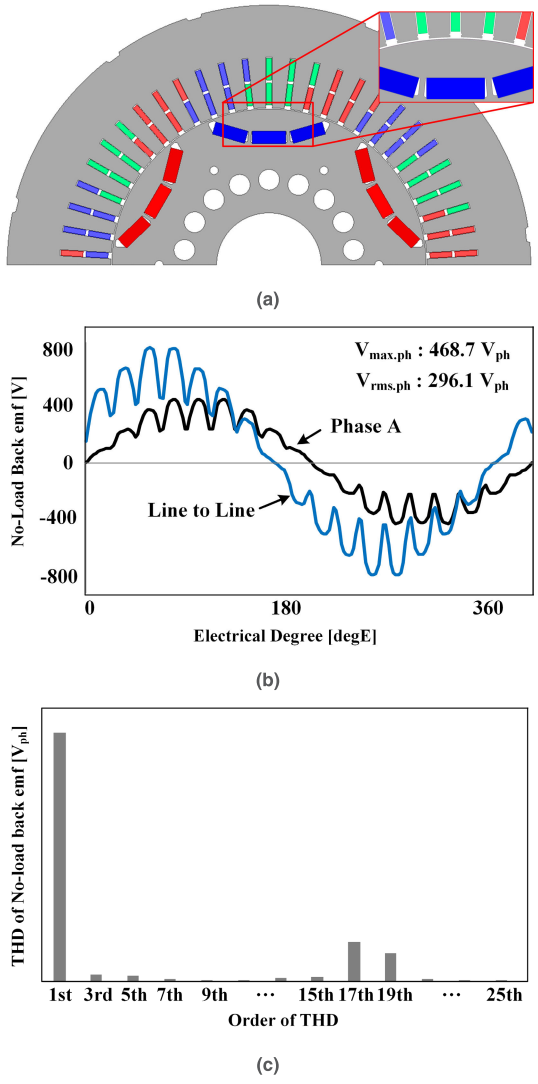

FIGURE 2. 140 kW IPMSM for urban railway traction motor: (a) 6-poles and 54-slots with slot-open (b) No-load back EMF wave form at 2200 rpm (c) THD of No-load phase back EMF.

parameters of a 140 kW IPMSM are shown in Table 1. A low current density was derived, as most of the heat generated from the motor was copper loss. Urban railway cars use a 7.07:1 reduction gear between the traction motor and the wheels. If the rotational speed of motor was 2200 rpm, which is also the rated speed, the vehicle speed was 48 km/h, and when it rotated at 4810 rpm, the vehicle speed was 105 km/h. The inverter frequency of the existing urban railway car is 800 Hz and the voltage is 1500 Vdc. The no-load back EMF waveform is required to be close to the sine waveform to secure controllability, as a 6-step control that requires accurate switching timing based on the rotor position is required after 3200 rpm, owing to limited switching frequency.

B. ANALYSIS OF NO-LOAD BACK EMF CHARACTERISTICS

Using a square winding has the advantage of increasing power density with a high fill factor. However, the rectangular winding needs a slot-open structure due to the manufacturing process. In other words, the width of the square wire should be smaller than the width of the slot. If a rectangular winding is used in the shoe structure as shown in Fig. 1(a), the hairpin technology must be applied [28]. The space slot harmonic component may not be large in case of an existing shoe shape as shown in Fig. 1(a). Conversely, in the slot-open structure, as there is no shoe part, and the slot opening is large, a very large space slot harmonic component is created. This space slot harmonic component is expressed by (1)

$$h_s = nq \pm 1 \quad (n = 1, 2, 3 \ldots) \tag{1}$$

where h_s is the space slot harmonics, n is the order of harmonics and q is the number of slot per pole pair.

Various space harmonic orders appear according to the stator permeance change as rotor rotating. This space harmonic component affects the magnetomotive force (MMF): hence, the MMF including the space harmonic component is represented as follows:

$$F_{pv} = \frac{1}{\pi}\int_{-\pi}^{\pi} f(x)\cos v\theta d\theta = \frac{4}{v\pi}\sin\frac{v\beta\pi}{2} \tag{2}$$

where F_{pv} is the magnetomotive force, v is the harmonic order and β is the short pitch angle.

According to (2), in order to minimize the space harmonics included in the MMF, a short pitch should be applied. However, there is a limit to reducing harmonics only by applying short pitch winding. Fig. 2(a) shows the structure of the 140 kW IPMSM with short pitch winding. As shown in Fig. 2(b), it can be observed that the harmonic components are large in the no-load back EMF waveform. As a result of the FFT analysis as shown in Fig. 2(c), the 17th harmonic is the largest. The fundamental magnitude of the no-load back EMF is 410.0 V, whereas the THD of the no-load back EMF is 20.8%. The THD is calculated as following:

$$THD = \frac{\sqrt{rms\ of\ back\ EMF^2 - rms\ of\ fundametal^2}}{rms\ of\ fundamental} \times 100\% \tag{3}$$

If the 17th harmonic is reduced, then the THD component of the no-load back EMF can be reduced, and the no-load back EMF waveform can be generated closer to the sine wave.

III. INVESTIGATION OF THE NOVEL SKEW ANGLE FOR THE SPECIFIC ORDER HARMONIC

The THD of no-load back EMF is related to a cogging torque and torque ripple [29]. There exists a traditional method of applying skew to the stator or rotor to reduce the no-load back EMF THD. In the traditional skew application method, the skew angle is calculated within one slot pitch angle. If the skew angle exceeds one slot pitch, the motor output decreases, and manufacturing becomes more difficult [30]. According to [31], [32], the traditional skew angle is derived as (4).

$$\theta_{skew} = \frac{2k\pi}{N_L} \quad [k = 1, 2, 3 \ldots] \tag{4}$$

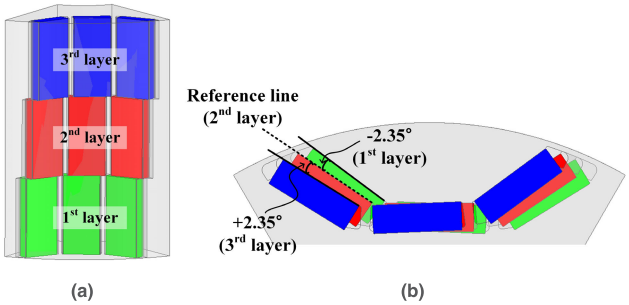

FIGURE 3. Three dimensional model of rotor with 3-layers step novel skew (a) front view (b) top view.

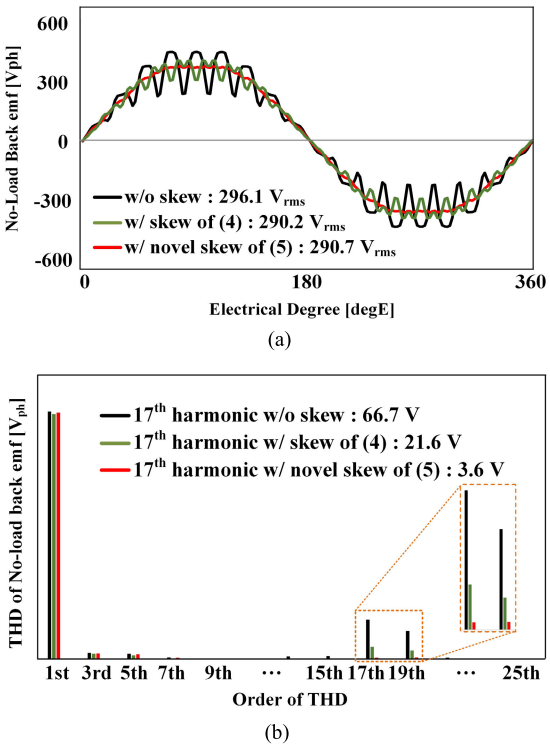

FIGURE 4. Comparison of no-load back EMF characteristics according to various skew angles at 2200 rpm: (a) Back EMF wave form (b) THD of no load back EMF.

where θ_{skew} is the skew angle and N_L is the least common multiple of the number of slots and poles.

In this study, a novel skew angle concept has been introduced to reduce harmonics of a specific order as follows:

$$n^{th}THD \times \theta_e = \frac{360}{N_{step}}$$
$$\theta_{skew\_adjacent} = \frac{\theta_e}{p}$$
$$\theta_{novel\_skew} = \theta_m \times (N_{step} - 1) \quad (5)$$

where θ_e is the electrical angle, θ_m is the mechanical angle, $\theta_{novel\_adjacent}$ is the skew angle with an adjacent stage, θ_{novel_skew} is the total novel skew angle and N_{step} is the number of step skew stages.

In (5), the left-hand side term of the first equation is multiplied by the electric angle of the harmonic order to be reduced, and the right term is divided by the number of step skew stages per rotor pole. The skew stages is divided to calculate the skew angle with each skew stage; in this study, three stages of step skew have been applied. The second line in (5) shows a formula to calculate the novel skew angle with the adjacent stage by dividing the electric angle by the number of pole pairs. The last line in (5) is an equation for calculating the total step skew angle.

This novel skew angle formula was created by considering the electrical and mechanical angles with respect to reduction in a specific harmonic order. As harmonics, cogging torque, and torque ripple all possess periodicity, the novel skew angle formula was derived from the relationship between the electrical cycle and the harmonic order. The skew angle for reducing the 17th harmonic was calculated; it was obtained as 4.7 degree. If the skew angle is calculated using (4), it is 6.7 degrees, which is equal to the pitch of one slot. In this study, a three-step skew was applied to the rotor to analyze the output characteristics when the skew angle was 4.7 degree as shown in Fig. 3. It is based on the second layer (reference line), which is the d-axis, whereas the first layer and the third layer were rotated by 2.35 degrees, respectively.

Applying the skew reduced the change in the reluctance between the stator and the rotor, which in turn reduced the spatial harmonics. Comparison of the no-load back EMF characteristics and cogging torque characteristics according to the skew angle of (4) and (5) is shown in Fig. 4. As a result of applying the skew using (4), the waveform was enhanced,

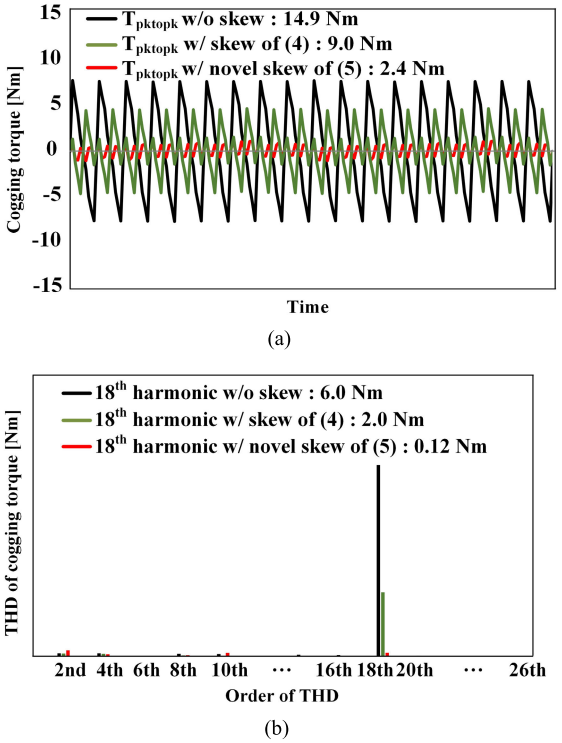

FIGURE 5. Comparison of cogging torque characteristics according to various skew angle at 2200 rpm (a) Cogging torque wave form (b) THD of cogging torque.

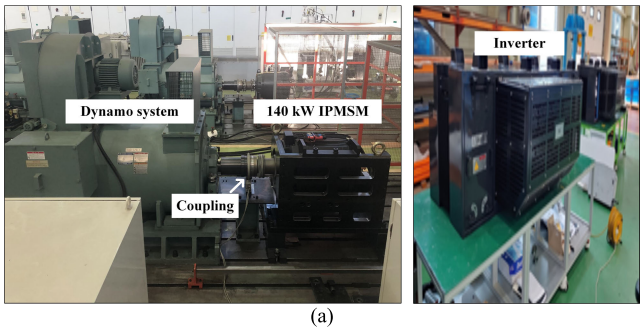

(a)

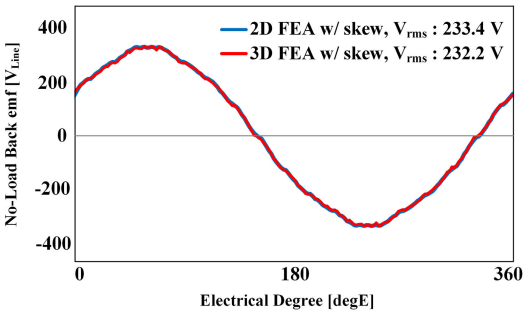

(b)

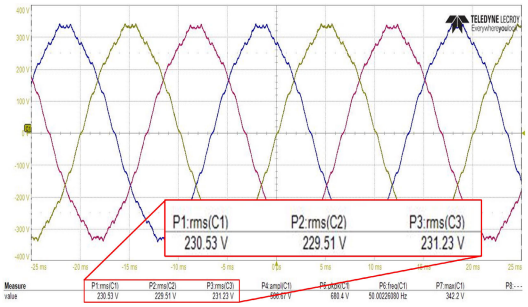

(c)

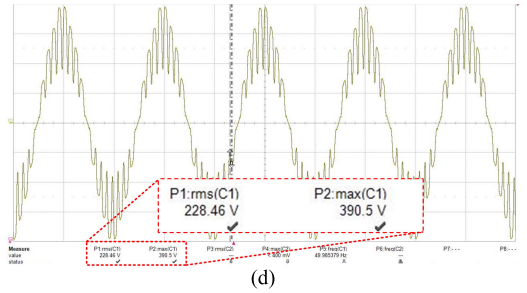

(d)

FIGURE 6. Experimental result @ 1000 rpm (a) Experimental setup of 140 kW IPMSM with the novel skew angle (b) 2D and 3D FEA results of no-load back EMF (line voltage) (c) Experimental result of no-load back EMF (line voltage) with the novel skew (d) Experimental result of no-load back EMF (line voltage) without skew.

and the 17th and 19th harmonics decreased compared to a non-skew model. As a result of applying the skew according to (5), the results obtained were much more improved than in (4). In this regard, Fig. 5 shows the analysis results for the cogging torque characteristics. The cogging torque harmonic is related to the no-load back EMF harmonic. As shown in Fig. 5(b), the 18th order of the cogging torque harmonic

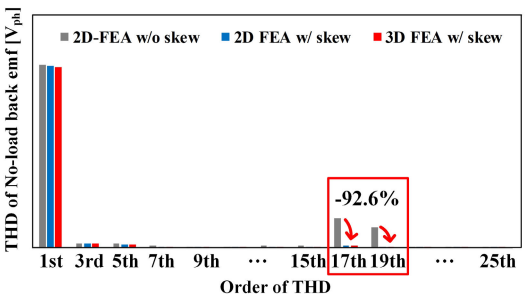

FIGURE 7. THD of no-load back EMF of non-skew and skew models.

is large because it was created by the 17th order 19th order of no-load back EMF THD, as explained in (6).

$$T = \frac{\sum_{n=odd} e_n i}{\omega_m}$$
$$T_{18} = \frac{E_{17} I}{\omega_m} \cos(18\omega t + \theta_{17}) + \frac{E_{19} I}{\omega_m} \cos(19\omega t + \theta_{19}) \quad (6)$$

In (6), e_n is the value of the nth no-load back EMF, which is the same as the characteristic of the no-load back EMF THD in Fig. 4(b). The no-load back EMF THD of the 17th order rotates in the same direction as the fundamental wave, whereas the no-load back EMF THD of the 19th order rotates in the opposite direction to the fundamental wave. Therefore, the 18th order torque ripple was reduced by offsetting each other.

To summarize the description of the novel skew angle, when the skew angle corresponding to one slot pitch was applied, the cogging torque waveform and the 18th harmonic of the cogging torque were relatively improved. More surprisingly, as a result of applying the novel skew angle, the cogging torque waveform was much improved as the 18th harmonic of the cogging torque was significantly reduced.

A prototype model with the novel skew angle of 4.7 degree was fabricated and an experiment was conducted. Fig. 6(a) illustrates the 140 kW IPMSM experiment, dynamo system, and the railway car inverter. Figs. 6(b) and 6(c) shows a comparison of the no-load back EMF waveform at 1000 rpm using 2-D and 3-D FEA and their experimental results, respectively. No-load back EMF wave was measured in the experiment of the prototype model without a skew angle, as shown in Fig. 6(d). The maximum speed of the measuring equipment was limited to 1000 rpm when measuring the no-load back EMF. On application of the novel skew angle, the no-load line back EMF waveform was enhanced. In Fig. 6(b), the graph lines are overlapped because there was no significant difference between the 2-D and 3-D FEA results. In addition, the measured value of back EMF between the no-load line through the experiment was about 230.4 Vline, and the 3-D FEA result was 232.2 Vline, showing an error of about 0.8%. The THD of the no-load back EMF based on the novel skew angle application, as shown in Fig. 7. The THD of the no-load back EMF decreased from 21.2% to 4.1% (based on 3-D analysis). As a result, it was confirmed that

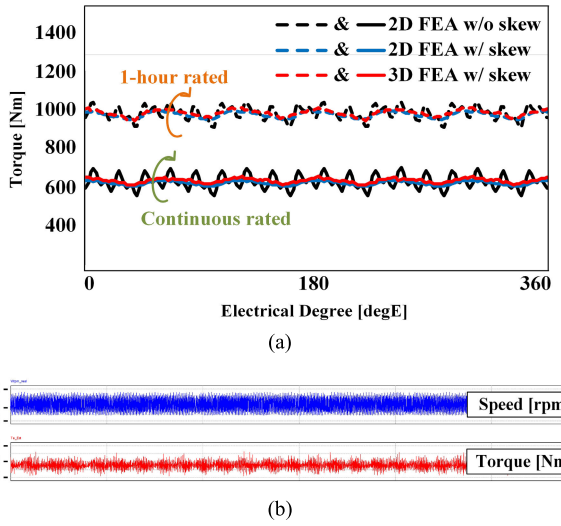

FIGURE 8. Comparison of torque at 2200 rpm with the novel skew model (a) Wave form of continuous and 1-hour rated torque by 2-D and 3-d FEA (b) Experimental result using a motor controller.

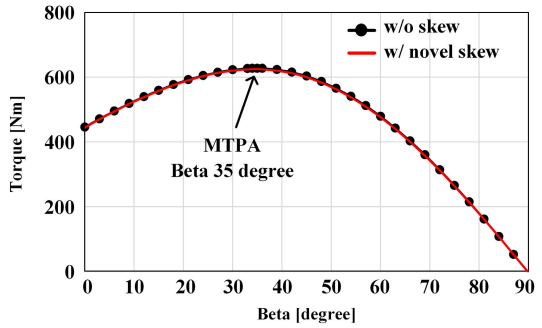

FIGURE 9. Torque trend by beta according to the novel skew at continuous rated @ 2200rpm by FEA result.

the 17th and 19th harmonics decreased by 92.6%, respectively. More importantly, even when the novel skew angle was applied, the no-load fundamental voltage reduced minimally by approximately 0.9% from 191.4 Vph to 189.7 Vph, indicating that reducing the motor output does not have a substantial effect.

IV. ANALYSIS OF OUPUT CHARACTERISTICS

As a result of analyzing the no-load back EMF characteristics in the previous section, it was confirmed that by applying the novel skew angle, the harmonics of a specific order are greatly reduced, while the fundamental voltage is minimally reduced. In the motor output characteristics, torque is a representative index representing the output, and the results of analyzing the torque with the application of the novel skew angle are shown in Figs. 8 to 10. When the switching frequency of the inverter of the railway car is limited to 800 Hz, SVPWM control is enabled up to 3200 rpm. This creates the requirement for a 6-step control after 3200 rpm. Therefore, it was performed with the current source, which conforms to SVPWM control at the rated speed of 2200 rpm. Additionally, it was performed with the voltage source in the same method as 6-step control

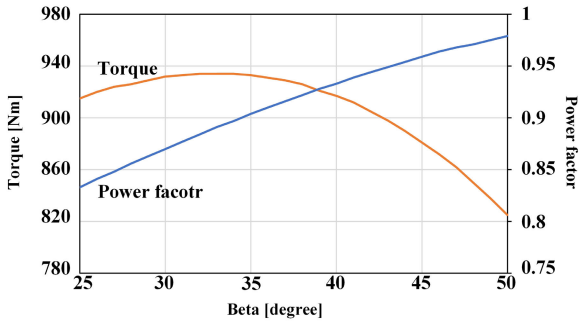

FIGURE 10. Torque and power factor at 1-hour rated condition by experiment.

at a maximum speed of 4810 rpm. In the SVPWM control, the phase voltage limit was 779 Vph.

The FEA results of the continuous rated, and 1 hour rated torque are shown in Fig. 8(a). After applying the novel skew angle, the average torque at the continuous rated decreased from 626.4 Nm to 620.4 Nm by approximately 6 Nm, based on 2-D FEA. Average torque of 3-D FEA was 632.1 Nm. The torque ripple decreased from 22.6% to 5.4% (2-D FEA) and 7.4% (3-D FEA). The average torque without the novel skew was 982.4 Nm at 1-hour rated condition; the average torque with the novel skew angle was 972.6 Nm (2-D FEA) and 982.3 Nm (3-D FEA). Fig. 8(b) shows the results of the experiment under continuous rated condition, the average torque here is 628 Nm.

Table 2 shows the results of comparison between the output characteristics, before and after the application of the novel skew angle. It can be observed that by applying the novel skew angle, differences in inductance and saliency were encountered. The core loss and solid loss were reduced due to the reduced flux linkage; however, the efficiency of the motor remained equal. Fig. 9 shows the results of the analysis of the torque in the continuous rated condition based on the novel skew. The average torque decreased slightly after applying the novel skew, but the torque trend and maximum torque per ampere (MTPA) point according to beta remained constant. This may be caused by the reduction of only the space harmonic components, while retaining the output characteristics. Fig. 10 shows the experimental result rated by the torque and power factor at 1-hour rated condition. The MTPA of the 1-hour rated condition is 32 degree and the power factor increased as the beta increased.

The average torque analysis result at the maximum speed is shown in Fig. 11. The voltage source corresponding to 6-step control was conducted at maximum speed. In the model without the novel skew angle, the average torque was 302.4 Nm and the torque ripple was 47.1%. Conversely, in the model with the novel skew angle, the average torque was 296.7 Nm, and the torque ripple was 32.6%, thus the novel skew angle resulted in a reduced torque ripple.

The electric steel sheet used in the 140 kW IPMSM is 30PNF1600 and the yield stress point of the material is 416 MPa. As shown in Fig. 11(b), the maximum load stress

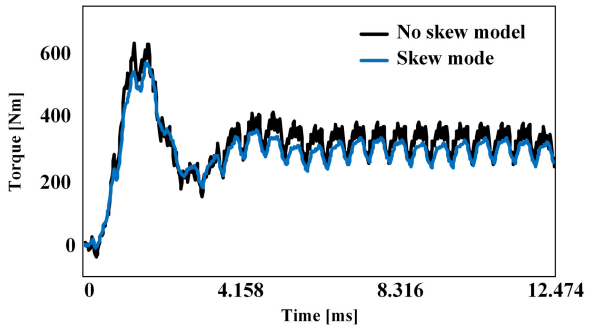

FIGURE 11. Torque wave form at 4810 rpm by 6-step control.

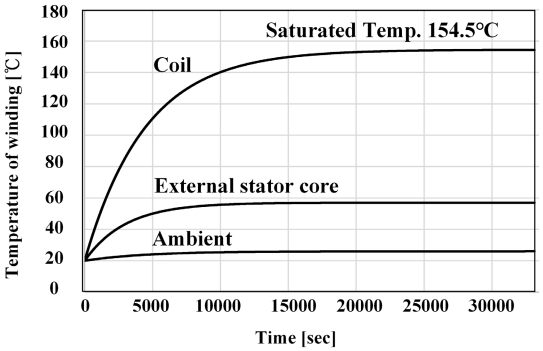

FIGURE 12. Motor temperature experiment result.

TABLE 2. Output characteristics of 140 kW IPMSM for urban railway traction motor.

Item	w/o skew model	w/ novel skew model
Linkage flux	0.949 Wb	0.948 Wb
Inductance of L_d	1.37166 mH	1.38051 mH
Inductance of L_q	6.21635 mH	6.15368 mH
Saliency rate	4.53	4.46
Beta	35 degree	35 degree
Average Torque	627.0 Nm	623.8 Nm
Core loss	1267.3 W	1266.9 W
Solid loss	31.1 W	30.4 W
Copper loss	1097.9 W	1097.9 W
Efficiency	98.4%	98.4%

of the final model is 278.88 MPa, which satisfies the required safety factor. Inner rib thickness acts as a key variable in strength analysis. When the outer and inner ribs become thicker, the safety factor improves, but the torque decreases due to the increase in the leakage of magnetic flux. In order to satisfy both the required torque and safety factor, the outer and inner rib must be at least 2 mm and 3.6 mm, respectively.

For a fully enclosed cooling system, the heat generation from copper loss is imminent. Copper loss can be expressed as shown in (7).

$$P_{copper\ loss} = 3I^2\rho\frac{l}{S} = 3I^2R\,[W] \tag{7}$$

TABLE 3. Mechanical analysis result of 140 kW IPMSM.

		Outer rib			T_{avg}
		1.8 mm	2.0 mm	2.2 mm	Safety factor
Inner rib	3.4 mm	628.8	625.8	623.6	Nm
		1.4	1.4	1.4	-
	3.6 mm	625.4	623.8	621.1	Nm
		1.4	1.5	1.5	-
	3.8 mm	622.6	620.8	618.3	Nm
		1.5	1.5	1.5	-

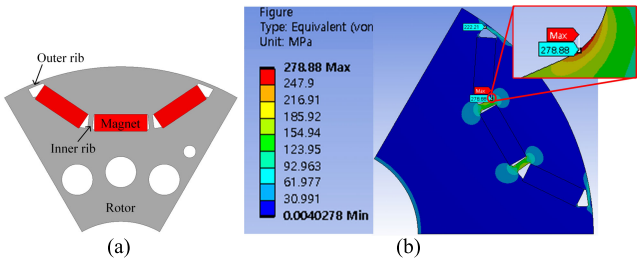

FIGURE 13. Mechanical analysis at 5770 rpm (a) key variable (b) result of final model.

where, ρ is resistivity of winding, l is the length of winding per phase and S is the area of the wire.

The current density was 2.84 A_{rms}/mm^2. Furthermore, the insulation class was manufactured based on a working temperature of 200°C. The cooling performance of the motor was dependent on the fan and internal structure of the housing. Fig. 12 shows the results of the temperature saturation experiment. The temperature sensor was installed on the stator winding, external stator core, and air. The ambient temperature of the experimental environment was about 20°C and the temperature saturation point was 154.5°C, resulting in a suitable result for a fully enclosed cooling system.

As permanent magnets are embedded in the rotor core of the IPMSM, the motor requires a design that prevents permanent magnets from scattering during high-speed rotation. In order to determine the presence of magnet scattering, mechanical analysis was performed under a condition of 5770 rpm. As shown in Fig. 13, the scattering of the magnets is determined based on the thickness of the outer and inner ribs of the rotor. Table 3 summarizes the results of the analysis of the average torque and the stress on the rotor according to the thickness of the outer and inner rib.

The safety factor required for a railroad vehicle towing motor is 1.5 and is calculated according to (8) [33].

$$Safety\ factor = \frac{Yield\ stress}{Max.\ load\ stress} \tag{8}$$

V. CONCLUSION

This study shows the design results of a traction motor in that accommodate a fully enclosed cooling system and the limited inverter switching frequency of urban railway cars. Most traction motor uses a square winding with a great fill factor for

high power density. However, as this type of winding requires a slot-open structure, the slot harmonic characteristics are considerably bad. Therefore, it adversely affects the THD of the no-load back EMF characteristics and torque ripple. A novel skew angle calculation method is proposed to reduce the harmonic of a specific order by analyzing the THD of the no-load back EMF.

In this study, the novel skew angle for reducing the 17th harmonic that has the biggest magnitude among the harmonics is 4.7 degree. The 2-D and 3-D FEA analysis was conducted by applying a three-step step skew to the rotor. As a result of applying the novel skew angle, the no-load back EMF waveform was improved, the 17th harmonic was reduced by 92.6%, and the torque ripple was also reduced by 67.3%, while the motor output minimally decreased. In order to validate the novel skew angle formula, a prototype model was fabricated by applying a fully enclosed cooling system, and the output characteristics from the FEA were verified through an experiment. Finally, a temperature saturation experiment was conducted that established that the temperature was saturated at 154.5°C. The cooling performance was thus verified to be excellent in terms of reliability.

REFERENCES

[1] R. Cao, E. Su, and M. Lu, "Comparative study of permanent magnet assisted linear switched reluctance motor and linear flux switching permanent magnet motor for railway transportation," *IEEE Trans. Appl. Supercond.*, vol. 30, no. 4, Jun. 2020, Art. no. 3601205.
[2] H. Lee, C. Park, and J. Lee, "Improvement of thrust force properties of linear synchronous motor for an ultra-high-speed tube train," *IEEE Trans. Magn.*, vol. 47, no. 11, pp. 4629–4634, Jun. 2011.
[3] H. Wang, J. Li, R. Qu, J. Lai, H. Huang, and H. Liu, "Study on high efficiency permanent magnet linear synchronous motor for maglev," *IEEE Trans. Appl. Supercond.*, vol. 28, no. 3, Apr. 2018, Art. no. 0601005.
[4] Y. J. Oh, J.-K. Lee, H.-C. Liu, S. Cho, J. Lee, and H.-J. Lee, "Hardware-in-the-loop simulation for active control of tramcars with independently rotating wheels," *IEEE Access*, vol. 7, pp. 71252–71261, 2019.
[5] Y. J. Oh, H.-C. Liu, S. Cho, J. H. Won, H. Lee, and J. Lee, "Design, modeling, and analysis of a railway traction motor with independently rotating wheelsets," *IEEE Trans. Magn.*, vol. 54, no. 11, Nov. 2018, Art. no. 8205305.
[6] Q. Xu, F. Ma, Z. He, Y. Chen, J. M. Guerrero, A. Luo, Y. Li, and Y. Yue, "Analysis and comparison of modular railway power conditioner for high-speed railway traction system," *IEEE Trans. Power Electron.*, vol. 32, no. 8, pp. 6031–6048, Aug. 2017.
[7] S. Nategh, H. Zhang, O. Wallmark, A. Boglietti, T. Nassen, and M. Bazant, "Transient thermal modeling and analysis of railway traction motors," *IEEE Trans. Ind. Electron.*, vol. 66, no. 1, pp. 79–89, Jan. 2019.
[8] J. Guzinski, M. Diguet, Z. Krzeminski, A. Lewicki, and H. Abu-Rub, "Application of speed and load torque observers in high-speed train drive for diagnostic purposes," *IEEE Trans. Ind. Electron.*, vol. 56, no. 1, pp. 248–256, Jan. 2009.
[9] S. Nategh, A. Boglietti, Y. Liu, D. Barber, R. Brammer, D. Lindberg, and O. Aglen, "A review on different aspects of traction motor design for railway applications," *IEEE Trans. Ind. Appl.*, vol. 56, no. 3, pp. 2148–2157, May 2020.
[10] B. Anton and A. Florescu, "Design and development of series-hybrid automotive powertrains," *IEEE Access*, vol. 8, pp. 226026–226041, 2020.
[11] H.-W. Lee, C.-B. Park, and B.-S. Lee, "Performance comparison of the railway traction IPM motors between concentrated winding and distributed winding," in *Proc. IEEE Transp. Electrific. Conf. Expo (ITEC)*, Dearborn, MI, USA, Jun. 2012, pp. 1–4.
[12] M. Torrent, J. Perat, and J. Jiménez, "Permanent magnet synchronous motor with different rotor structures for traction motor in high speed trains," *Energies*, vol. 11, no. 6, Jun. 2018, Art. no. 1549.
[13] D. Yu, X. Y. Huang, Y. T. Fang, and J. Zhang, "Design and comparison of interior permanent magnet synchronous traction motors for high speed railway applications," in *Proc. IEEE Workshop Electr. Mach. Design, Control Diagnosis (WEMDCD)*, Nottingham, U.K., Apr. 2017, pp. 58–62.
[14] M. Kondo, R. Ebizuka, and A. Yasunaga, "Rotor design for high efficiency induction motors for railway vehicle traction," in *Proc. Int. Conf. Electr. Mach. Syst.*, Tokyo, Japan, Nov. 2009, pp. 1–4.
[15] S. Nategh, D. Lindberg, R. Brammer, A. Boglietti, and O. Aglen, "Review and trends in traction motor design: Electromagnetic and cooling system layouts," in *Proc. 13th Int. Conf. Electr. Mach. (ICEM)*, Alexandroupoli, Greece, Sep. 2018, pp. 2600–2606.
[16] E. Yolacan, M. K. Guven, M. Aydin, and A. M. El-Refaie, "Modeling and experimental verification of an unconventional 9-phase asymmetric winding PM motor dedicated to electric traction applications," *IEEE Access*, vol. 8, pp. 70182–70192, 2020.
[17] H.-J. Park and M.-S. Lim, "Design of high power density and high efficiency wound-field synchronous motor for electric vehicle traction," *IEEE Access*, vol. 7, pp. 46677–46685, 2019.
[18] K. Matsuoka, M. Kondo, and Y. Shimizu, "A totally enclosed traction motor using a permanent magnet synchronous motor," *Electr. Eng. Jpn.*, vol. 151, no. 3, pp. 71–80, 2005.
[19] H.-C. Liu, H.-J. Lee, H.-S. Seol, S. Cho, J. Lee, and Y. J. Oh, "Optimal slot design of IPMSM in railway with independently rotating wheelsets," *IEEE Trans. Magn.*, vol. 55, no. 2, Feb. 2019, Art. no. 8200404.
[20] Z. Q. Zhu, Y. Liu, and D. Howe, "Minimizing the influence of cogging torque on vibration of PM brushless machines by direct torque control," *IEEE Trans. Magn.*, vol. 42, no. 10, pp. 3512–3514, Oct. 2006.
[21] D.-S. Jung, Y.-H. Kim, U.-H. Lee, and H.-D. Lee, "Optimum design of the electric vehicle traction motor using the hairpin winding," in *Proc. IEEE 75th Veh. Technol. Conf. (VTC Spring)*, Yokohama, Japan, May 2012, pp. 1–4.
[22] S. Wang, J. Hong, Y. Sun, and H. Cao, "Effect comparison of zigzag skew PM pole and straight skew slot for vibration mitigation of PM brush DC motors," *IEEE Trans. Ind. Electron.*, vol. 67, no. 6, pp. 4752–4761, Jun. 2020.
[23] X. Bao, J. Fang, C. Di, and S. Xu, "A novel computational method of skewing leakage reactance for a doubly skewed rotor induction motor," *IEEE Trans. Energy Convers.*, vol. 33, no. 4, pp. 2174–2182, Dec. 2018.
[24] H. Wu, P. Wu, K. Xu, J. Li, and F. Li, "Research on vibration characteristics and stress analysis of gearbox housing in high-speed trains," *IEEE Access*, vol. 7, pp. 102508–102518, 2019.
[25] S. S. R. Bonthu, T. B. Tarek, and S. Choi, "Outer rotor permanent magnet synchronous reluctance motors," *IEEE Trans. Energ. Convers.*, vol. 33, no. 3, pp. 1184–1192, Sep. 2018.
[26] P. Lazari, J. Wang, and B. Sen, "3-D effects of rotor step-skews in permanent magnet-assisted synchronous reluctance machines," *IEEE Trans. Magn.*, vol. 51, no. 11, pp. 1–4, Nov. 2015.
[27] Y. Kawase, T. Yamaguchi, Z. Tu, N. Toida, N. Minoshima, and K. Hashimoto, "Effects of skew angle of rotor in squirrel-cage induction motor on torque and loss characteristics," *IEEE Trans. Magn.*, vol. 45, no. 3, pp. 1700–1703, Mar. 2009.
[28] T. Ishigami, Y. Tanaka, and H. Homma, "Motor stator with thick rectangular wire lap winding for HEVs," *IEEE Trans. Ind. Appl.*, vol. 51, no. 4, pp. 2917–2923, Jul./Aug. 2015.
[29] H. Jang, H. Kim, H.-C. Liu, H.-J. Lee, and J. Lee, "Investigation on the torque ripple reduction method of a hybrid electric vehicle motor," *Energies*, vol. 14, no. 5, Mar. 2021, Art. no. 1413.
[30] D. Barman and P. Pillay, "Effect of skewing in a variable flux interior permanent magnet synchronous machine," *IEEE Trans. Ind. Appl.*, vol. 56, no. 6, pp. 6399–6410, Nov. 2020.
[31] L. Zhu, S. Z. Jiang, Z. Q. Zhu, and C. C. Chan, "Analytical methods for minimizing cogging torque in permanent-magnet machines," *IEEE Trans. Magn.*, vol. 45, no. 4, pp. 2023–2031, Apr. 2009.
[32] X. Ge, Z. Q. Zhu, G. Kemp, D. Moule, and C. Williams, "Optimal step-skew methods for cogging torque reduction accounting for three-dimensional effect of interior permanent magnet machines," *IEEE Trans. Energy Convers.*, vol. 32, no. 1, pp. 222–232, Mar. 2017.
[33] H. Jang, S.-T. Oh, Y. Park, H. Kim, I. S. Jang, and J. Lee, "Design and analysis of a novel rotor shape to improve power performance," *IEEE Trans. Appl. Supercond.*, vol. 30, no. 4, Jun. 2020, Art. no. 5201304.

HYUNGKWAN JANG received the B.S. and M.S. degrees in electrical engineering, and the Ph.D. degree in design algorithm development of high efficiency and power density synchronous motors for traction and home appliance from Hanyang University, Seoul, South Korea, in 2010, 2012, and 2021, respectively. He worked at LG Electronics, from 2013 to 2017. He is currently working as a Postdoctoral Researcher with Hanyang University. His research interests include design, analysis of motor/generator, which are applied in mechanical and electrical systems in railway cars, electric vehicles, automotive parts, and home appliance.

HYUNWOO KIM received the B.S. and M.S. degrees in electrical engineering from Hanyang University, Seoul, South Korea, in 2017 and 2019, respectively, where he is currently pursuing the Ph.D. degree in design algorithm development of high efficiency and power density synchronous motors. His research interests include design, analysis, and control drives of motor/generator, which are applied in mechanical and electrical systems in electric vehicles and automotive parts.

DONG-WOO NAM received the B.S. and M.S. degrees in energy IT from Gachon University, Seongnam-si, South Korea, in 2019 and 2021, respectively, where he is currently pursuing the Ph.D. degree with the Department of Electric Engineering. His research interests include design and analysis of motors/generators, which are applied in vehicles, home appliances, and industrial electrical machinery.

WON-HO KIM received the B.S., M.S., and Ph.D. degrees in electrical engineering from Hanyang University, Seoul, South Korea, in 2005, 2007, and 2011, respectively.

From 2011 to 2017, he was a Research Staff Member with Samsung Advanced Institute of Technology, Yongin-si, South Korea. Since 2017, he has been an Assistant Professor with the Electrical Engineering Department, Gachon University, Seongnam-si, South Korea. His research interests include design and analysis of motors/generators, which are applied in vehicles, home appliances, and industrial electrical machinery.

JU LEE (Senior Member, IEEE) received the B.S. and M.S. degrees in electrical engineering from Hanyang University, Seoul, South Korea, in 1986 and 1988, respectively, and the Ph.D. degree in electrical engineering from Kyusyu University, Japan, in 1997. He joined Hanyang University, in 1997, where he is currently a Professor with the Division of Electrical and Biomedical Engineering. His main research interests include electric machinery and its drives, electro-magnetic field analysis, and transportation systems, such as hybrid electric vehicles (HEV) and railway propulsion systems. He is a member of the IEEE Industry Applications Society, the Magnetics Society, and the Power Electronics Society.

CHANGSUNG JIN received the B.S., M.S., and Ph.D. degrees from Hanyang University, Seoul, South Korea, in 2001, 2003, and 2011, respectively. He joined Wonkwang University, Iksan, South Korea, in 2018, where he is currently a Professor with the Division of Electrical Engineering. His main research interests include design of electric machinery, electro-magnetic field analysis, hybrid electric vehicle (HEV) and electric vehicle (EV), home appliance, and solar photovoltaics (PV).